Composites Science and Technology 181 (2019) 107701

Contents lists available at ScienceDirect

Composites Science and Technology

journal homepage: www.elsevier.com/locate/compscitech

High-strength and physical cross-linked nanocomposite hydrogel with clay nanotubes for strain sensor and dye adsorption application

Keying Feng[1], Guang-Yu Hung[1], Xiaohan Yang, Mingxian Liu*

Department of Materials Science and Engineering, Jinan University, Guangzhou, 510632, PR China

ARTICLE INFO

Keywords:
Nanoclays
Nano composites
Strength
Scanning electron microscopy (SEM)
Casting

ABSTRACT

A high-strength nanocomposite hydrogel composed with polyacrylamide (PAAm) is fabricated via in-situ free radical polymerization of acrylamide in presence of halloysite nanotubes (HNTs) and then by ethanol immersing. HNTs act as physical cross-linkers for PAAm chains via hydrogen bonding interactions, while ethanol makes the crosslinking network denser by release of water. The mechanical properties of hydrogels are significantly increased by addition of HNTs and ethanol treatment. The structure of the composite hydrogel was studied by Fourier-transform infrared spectroscopy (FTIR), scanning electron microscopy (SEM), and X-ray diffraction (XRD). Interestingly, the composites hydrogels show good conductivity, which is attributed to the presence of the potassium ion in hydrogel network originated from initiator. Therefore, the composite hydrogels can be applied in strain sensor, which can monitor human activities such as bending and releasing the finger, elbow, knee as well as detecting walking pace with high sensitivity. Moreover, the freeze-dried gels show superior removal efficiency of methylene blue dye from water in short time. This work developed a simple, economical, and practical way to synthesize high-strength nanocomposite hydrogel using natural nanotubes, which shows promising applications in strain sensor and environmental restoration.

1. Introduction

Hydrogel is a kind of cross-linked polymer with three-dimensional network structure, which can swell in water and retain a large amount of water but cannot be dissolved [1]. The hydrogels can be divided into natural hydrogels and synthetic hydrogels according to materials source [2]. Natural hydrogels such as collagen [3], fibrin [4], chitosan [5], cyclodextrin [6], and dextrin [7] display good biocompatibility and biodegradability, however, they always have poor mechanical property. Synthetic hydrogels show high mechanical strength, which are cross-linked polymers prepared by polymerization in presence of water. The traditional chemical cross-linked hydrogel has certain defects. For example, when the degree of cross-linking is high, the hydrogels exhibit low water absorption (dehydration) rate and low strength as well as brittleness. This limits the practical application in daily life and industry. In contrast, the physically crosslinked hydrogel is expected to be highly flexible with high toughness, which can meet the application in tissue engineering, artificial muscles, separations technology, sensor and so on [8–10]. The physical crosslinking method includes ionic interactions, crystallization, hydrophobic interactions, and hydrogen bonding interactions. Haraguchi firstly developed a polyacrylamide (PAAm) nanocomposite hydrogel with extraordinary mechanical, optical, and swelling properties using layered hectorite as filler and crosslinking agent [11]. The physically crosslinked network can also combine with chemically crosslinked network to synergistically enhance the performance of polymer hydrogel. For example, alginate/PAAm double-network hydrogel was prepared with Ca^{2+} crosslinked alginate as the first network and chemically crosslinked PAAm as the second network [12,13]. The tensile strength and strain at rupture of the hydrogel were 156 KPa and 2300%, while the fracture energy was up to 9000 J/M^2. More importantly, the physical cross-linked hydrogels can be self-healing materials since new bond can be formed through the reconstruction of non-covalent hydrogen bonding. Exploring proper nanoparticles especially from natural sources with strong interfacial interactions with polymer chains is one of the key tasks to prepare high-strength nanocomposite hydrogel.

Halloysite nanotubes (HNTs) are 1:1 natural aluminosilicate clay mineral with the chemical formula $Al_2Si_2O_5(OH)_4.nH_2O$ [14]. The typical morphology of halloysite is tubular structure with empty lumen. The inner diameter, outer diameter, and length of HNTs are in the range of 10–20 nm, 40–70 nm, and 200–1500 nm, respectively [13]. Different to other clays, most Al–OH groups of halloysite are located in the

* Corresponding author.
E-mail address: liumx@jnu.edu.cn (M. Liu).
[1] These authors contributed equally to this work.

https://doi.org/10.1016/j.compscitech.2019.107701
Received 5 May 2019; Received in revised form 17 June 2019; Accepted 23 June 2019
Available online 25 June 2019

innermost surfaces, while the outer surfaces are mainly Si–O groups. Also, small amount of Si–OH and Al–OH groups exposed at the edges of the tubes. Interestingly, the outer and inner surfaces of HNTs are negatively charged and positively charged, respectively [15]. Owing to the unique tubular structure and surface hydroxyl groups, the clay shows promising application in composite and biomaterials such as drug controlled release [16–18] and capture of tumor cells [19], adsorption of pollutants from water [20–22], catalyst carrier [23,24]. As reinforcing filler, halloysite can be mixed in melt with polyolefin [25], polyurethane [26], and natural rubber [27]. HNTs have also been used for fabricating nanocomposite hydrogels [28–30]. For example, we prepared sodium alginate/HNTs composite hydrogels by solution blending and cross-linking with calcium ions, where HNTs improve the physical properties and cytocompatibility of composite hydrogels significantly [31]. A tri-component hydrogel composed with gellan gum, glycerol, and HNTs also exhibits improved biocompatibility and potential for incorporation of target biomolecules [32]. The features of low price, high strength, large aspect ratio, biocompatibility, easy surface modification and controlled release properties make HNTs show promising application in hydrogel.

Strain sensors are devices which can transduce mechanical deformations into electrical signals. Strain sensors have broad applications in health-monitoring, mass measurement, pressure sensing, sports performance monitoring, human-machine interfaces and so on [33]. Most flexible strain sensors are fabricated with composite [34], which based on the conductive materials such as metal particles [35], ion [36], carbon nanotube [37], graphene [38] or conductive polymer [39]. Hydrogel has become a promising material for strain sensor due to its stretchable, wearable, flexible, sensitive, and human friendly performance. Various methods have been developed for the preparation of hydrogel for strain sensor application. For example, Wang et al. developed tough conductive hydrogels composed of interpenetrating polyaniline and poly(acrylamide-*co*-hydroxyethyl methyl acrylate) networks [40]. These conductive hydrogels showed high sensitivity (gauge factor 11), but the fracture strain decreased sharply with the increasing oxidation time of the aniline. Jing et al. reported a multifunctional hydrogel synthesized by incorporating polydopamine-coated talc nanoflakes into PAAm [41], which could be rapidly self-healed and regain its mechanical properties without external stimuli. It also showed high sensitivity as a strain sensor with a gauge factor of 0.693 at 1000% strain. However, the fabrication method of these composite hydrogel is complicated, and the sensitivities of the sensor are not satisfied. Also, large ratio of conductive nanomaterials should be added into the polymer strain sensors.

Here, we constructed high-strength nanocomposite hydrogels for strain sensor. The hydrogels are fabricated via in-situ free radical polymerization of acrylamide in an aqueous suspension of HNTs and then by ethanol immersing. HNTs act as cross-linking agent of PAAm, while ethanol immersion shrinks the network of hydrogels and enhances the interactions between HNTs and PAAm. The tensile strength increased from 74 KPa to 234 KPa, accompanied by the elongation at break from 885% to 2083% after the treatment in anhydrous ethanol. Owing to the ionic transport, the prepared hydrogels with superior mechanical properties are conductive, and the strain sensors made by the hydrogel can monitor the movement of fingers, elbows, knees and even pace speed. In addition, the dried hydrogel can adsorb dye from water effectively. Since the preparation method is simple and raw materials are cheap, the PAAm-HNT composite hydrogel shows promising application as strain sensor and sewage treatment agent.

2. Experimental

Materials. Potassium peroxydisulfate ($K_2S_2O_8$, > 99.5%) was purchased from Tianjin baishi chemical co. LTD. Acrylamide (C_3H_5NO, > 99.0%) was purchased from Aladdin. Anhydrous ethanol (CH_3CH_2OH, ≥99.7%) was used without any treatment. HNTs were purchased from Guangzhou Runwo Materials Technology Ltd., China. The elemental composition of HNTs determined by X-ray fluorescence (XRF) was as follows (wt.%): SiO_2, 58.91; Al_2O_3, 40.41; Fe_2O_3, 0.275; TiO_2, 0.071. Laponite-RD was purchased from BYK. The diameter of glass tube was 10 mm.

Preparation of PAAm-HNT composite hydrogels. The composite hydrogels were prepared via in-situ radical polymerization in the HNTs aqueous dispersion system. First, 4 g HNTs without purification were added to 20 mL pure water and dispersed for 1–2 h to ensure uniform dispersion. Then 3 g AAm was added and stirred at room temperature for 30 min. After 3 mL 20 wt% KPS solution was added to the mixture, the solution was stirred well and quickly poured into glass tube with diameter of 10 mm. The polymerization reaction then occurred in the oven at 60 °C for 3 h. The weight percentage of HNTs in the final composite was 14.8%. Next, the PAAm-HNT hydrogels were soaked in ethanol for different time. The percentage of the ethanol stood for the volume ratio of ethanol to water. The pure PAAm hydrogel was also synthesized with similar procedures but without the addition of HNTs. The trace amount of bisacrylamide in AAm could act as the crosslinking agent for pure PAAm hydrogel.

2.1. Characterization

Mechanical performance testing. The tensile properties of PAAm-HNT composites were tested using a universal testing machine (UTM-Q422, China Chengde Jinjian Testing Instrument Co., Ltd.) at a tensile rate of 50 mm/min.

Rheological property. The rotating rheometer (Kinexus pro +, Malvern Instruments, Malvern, UK.) was used to measure the dynamic viscosity of PAAm-HNT hydrogels at room temperature. A parallel plate with a diameter of 15 mm was chosen and the gap between the two parallel plates was 1 mm. First, the dynamic strain scan was performed from 0.1% to 100% at fixed angular frequency of 1 Hz, and then the frequency scan was performed from 0.1 to 100 Hz when the strain was fixed at 0.5%.

Morphology. The surface of the fractured freeze-dried hydrogel was observed using a scanning electron microscope (Zeiss Ultra 55 SEM, KYKY Technology Co., LTD, China). The voltage of the electron beam was set at 5 kV.

FTIR. The FTIR spectra of the HNTs and the freeze-dried hydrogels was conducted on FTIR Spectrometer (Nicolet iS50 FT-IR, Thermo Scientific, USA). Thirty-two consecutive scans were taken and their average was stored. Spectra were taken from 4000 to 500 cm^{-1} at resolution of 2 cm^{-1}.

XRD. XRD spectrum of PAAm-HNT was obtained using X-ray diffractometer (D8, Bruker corporation, Germany) at room temperature. The CuKα radiation source was operated at 40 kV power and 40 mA current. The wavelength of the X-ray beam was 0.15418 nm, and the scanning angle was from 5° to 60°.

Volume shrinkage and swelling properties. The volume shrinkage of hydrogel was calculated by the equation of

$$\text{Shrinkage ratio} = \frac{(V_0 - Vx)}{V_0} \times 100\%$$

where V_0 referred to the volume of hydrogel without soaking anhydrous ethanol, and V_x was the volume after soaking anhydrous ethanol for 10 min, 30 min, 1 h, 2 h and 24 h. Swelling rate of the prepared hydrogels was calculated from equation of

$$\text{Swelling ratio} = \frac{M_1 - M_0}{M_0} \times 100\%$$

where M_0 was the initial mass and M_1 was the mass after a 24 h immersion in water.

Conductivity. The conductivity of the hydrogels was measured using a multimeter (Fluke 17B+, R > 2 × 108 Ω, China). The resistance of the sample was measured by two-point method.

Adsorption Measurements. The adsorption ability of freeze-dried hydrogels toward methylene blue (MB) was investigated. First, 50 mg L^{-1} MB solution was prepared by stirring. To investigate the effect of adsorption time on adsorption capacity of the freeze-dried hydrogels, 1.2 g freeze-dried hydrogels was immersed into a container with 25 mL MB solution (50 mg L^{-1}). The swelling hydrogels and solution were separated by filtration, and the absorbance of filtrate of different adsorption time was measured by ultraviolet spectrophotometer (UV-2550, Shimadzu Instrument Ltd., Suzhou, China) from 450 nm to 750 nm wavelength. The adsorption capability (Q_t) and removal efficiency (E) of the freeze-dried hydrogels were calculated according to the following formula:

$$Q_t = \frac{(C_0 - C_t) \times V_0}{m} \quad E = \frac{C_0 - C_t}{C_0}$$

Where Q_t represented the adsorption capacity at time t, C_0 (50 mg L^{-1}) and C_t represented the concentration of MB solution before and after being adsorbed for a certain time (t), respectively, while m (1.2 g) and V_0 (25 mL) represent the mass of composite hydrogel and the initial volume of MB solution, respectively.

3. Results and discussion

3.1. Mechanical properties

First, a dispersion composed of acrylamide and HNTs was prepared by stirring. With potassium persulfate as the initiator, the nanocomposite hydrogels were prepared via in-situ free radical polymerization of acrylamide in the presence of HNTs. The hydrogen atom of silanol on the surface of HNTs can form hydrogen bond with amide group of PAAm which has been confirmed by our previous study [42]. Meanwhile, there are also certain hydrogen bonds and segment entanglement among the molecular chains of PAAm. Due to the high viscosity of the solution, some bubbles cannot be totally removed and stay inside the hydrogels. Surprisingly, ethanol immersion could solve this problem as some bubbles are attached on the surface of hydrogels during this process, which is beneficial to the elimination of the defects of the hydrogels. Ethanol immersion can also remove un-crosslinked free PAAm chains as well as remaining monomer to some degree. After being soaked in ethanol, the gel network shrinks and the structure becomes densified. The elimination of bubbles insides the hydrogels and the increase in the interactions of hydrogen bond and entanglement of chain segments lead to a more uniform physical-crosslinking network. When the hydrogels are stretched, part of the hydrogen bonds are sacrificed to dissipate energy while the unbroken hydrogen bonds play the critical role in the recovery of the strain. Therefore, the process of ethanol immersion can greatly enhance the mechanical properties of hydrogels. The preparation process and the reinforcing mechanism of the PAAm-HNT composite hydrogel are shown in Fig. 1.

It is found that both pure PAAm hydrogel and PAAm-HNT hydrogel exhibit improved toughness and strength after the treatment of ethanol immersion. As shown in Fig. 2A, the elongation at break and the tensile strength of pure PAAm hydrogel are 286% and 31 KPa, respectively. After the immersion in anhydrous ethanol for 1 h, the elongation at break and the tensile strength reach to 1008% and 66 KPa, respectively. Significant reinforcement can also be observed in PAAm-HNT hydrogel. The tensile strength of the hydrogel increases from 74 KPa to 234 KPa accompanied by the elongation at break from 885% to 2083% after the treatment in anhydrous ethanol. From the insert in Fig. 2A, the PAAm-HNT hydrogel has volume shrinkage after immersing in ethanol. Further study shows that both ethanol concentration and soaking time have great influence on the tensile properties. When the immersing time was kept for 1 h, the tensile modulus and the tensile strength of the hydrogel gradually improved with increase in ethanol concentration. Meanwhile, the elongation at break increases initially as ethanol concentration increases and then decreases afterwards, as shown in Fig. 2B.

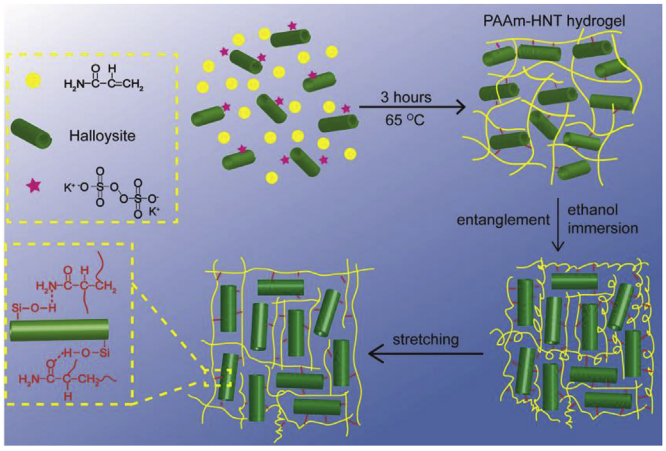

Fig. 1. Schematic illustration of the preparation process of the high-strength PAAm-HNT nanocomposite hydrogel.

A highest elongation of 2710% is obtained at the ethanol concentration of 75%, and a highest tensile strength of 235 KPa is obtained at the ethanol concentration of 100%.

Similar results can be seen by immersing the samples in anhydrous ethanol for different time (Fig. 2C–D). The tensile strength gradually improves as the immersing time increase. With an immersion time of 4 h, the surfaces of the samples are smooth and the tensile strength reach to 382 KPa. Although the tensile strength of hydrogels reaches to 4.5 MPa with an immersion time of 24 h, the gels have already become stiff and rigid with many wrinkles on the surfaces. The elongation at break reaches to the maximum of 2083% with an immersion time of 1 h, and then decreases with longer immersion time. From the tensile properties above, it can be concluded that the treatment of ethanol immersion can provide a perfect reinforcement for the PAAm-HNT hydrogels. The increase of mechanical properties is almost proportional to the loading of HNTs, but it's hard to obtain a composite hydrogel with more than 30% HNTs [42].

Here we explored a new way to prepare high-strength composites hydrogel by immersing the hydrogels in anhydrous ethanol and proposed the reinforcing mechanism. Due to the concentration difference of water content inside and outside the hydrogels, water in the hydrogels rapidly diffuse to the anhydrous ethanol. The gels shrink, defects like bubbles eliminate, and more entanglement occurrs among the PAAm upon with the water diffusion. Meanwhile, the chain segment of PAAm stick to the surface of HNTs to form a strong interface, which makes it more effective to transfer the loading between PAAm and HNTs. All of these account for the improved strength. If one treated the hydrogels with acetone or other polar organic solvent, the strength of the hydrogels would also increase. Previous studies also provided this similar mechanism. For example, the chemically cross-linked chitin or cellulose gels were immersed into the desired concentration of aqueous ethanol to form physically cross-linked domains through hydrogen bonding, hydrophobic interactions, and crystalline hydrates formation. The chemical and physical cross-linking lead to the biological hydrogel with super strength and toughness. However, this method has not been used in PAAm hydrogel systems. It's reported that HNTs play the role of physical cross-linking points for PAAm chain. The polymer chains which anchored on the HNTs surfaces via physical interactions can be slipping along the tube during the tensile testing [42].

The composite hydrogels can undergo many loading-underloading cycles without broken, and the polymer chains can be stretched by the stress for many times. These facts lead to the increased extensibility for the PAAm-HNT hydrogels. The reinforcing mechanism by ethanol immersing is also suitable for the PAAm-Laponite composite hydrogels, as shown in Fig. S1. However, the increase of the strength and the elongation at break are not always synchronous, which depends on the

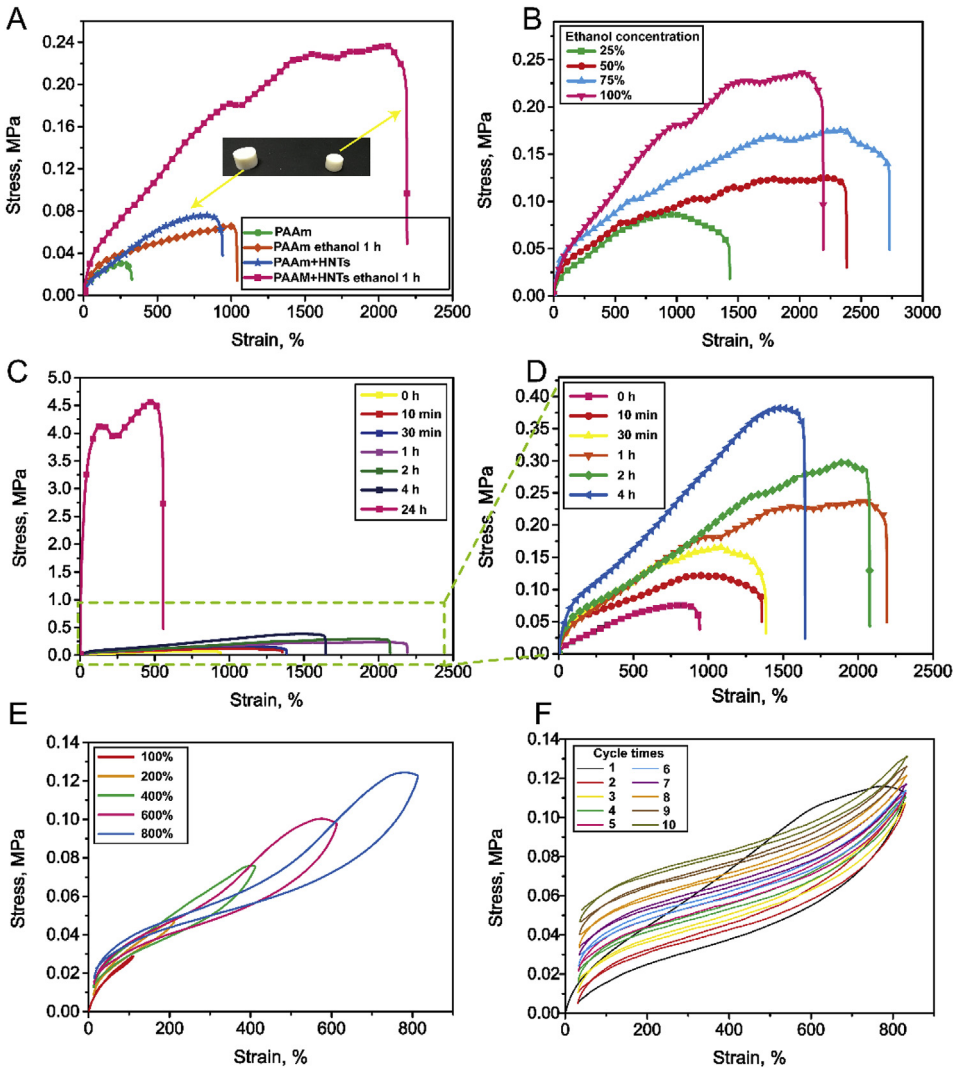

Fig. 2. Tensile properties of the hydrogels. A) Stress-strain curves of PAAm hydrogel and the PAAm-HNT hydrogel before and after ethanol immersion. The inset shows the appearance of the PAAm-HNT hydrogel before and after ethanol soaking. Tensile properties of PAAm-HNT hydrogel treated with B) different ethanol concentration, C) different immersion time. D) Stress-strain curves of the PAAm-HNT hydrogel with ethanol immersion time from 0 h to 4 h. E) The stress-strain curves for elongation-recovery of PAAm-HNT hydrogel with increasing strain from 100% to 800%. F) The stress-strain curves for elongation-recovery of PAAm-HNT hydrogel at the strain of 800% for 10 times.

interfacial strength between PAAm and HNTs and the structure of the hydrogels. At relatively long immersion time and high ethanol concentration, numerous hydrogen bonding between PAAm and HNTs and complex chain entanglement result in tight hydrogels network and enhanced strength. This process usually makes contribution to the tensile strength but do harm to the mobility of the chain segment. It's difficult for the chain segment to move when the network is too tight and the interfacial interaction is too strong. Therefore, the gels become fragile with long immersion time or high immersion concentration (Fig. 2D).

As shown in Fig. 2E, although there is visible residual strain after a stretching-releasing cycle, the hysteresis cycles are very narrow. Fig. 2F furthered shows that the stress-strain curves are nearly overlapped apart from the first cycles. And it's probably brought by the lubrication effect of water in the gels network, which significantly reduces the resistance among chain segments. This phenomenon suggests the good elasticity of PAAm-HNT hydrogels. It should be also noted that the gels remain unbroken after 10 cycle tests, demonstrating a good fatigue resistance [43]. The hydrogels become rigid with the increasing cycle times which is mainly attributed to the increased alignment of the macromolecular chains and the volatilization of ethanol or water in gels during the tensile process.

As shown in Fig. 3A_1-A_4, the PAAm-HNT hydrogels exhibit superior extensibility. The knotted gels with an initial length of 5 cm can be stretched to 8 times or even more. In addition, the gels can also lift 600 g of the steel block or the 330 mL of the Coca Cola without any rupture (Fig. 3B and C). To study the volume shrinkage, the PAAm-HNT hydrogels were soaked into a large amount of anhydrous ethanol for different time. As shown in Fig. 3D, the volume shrinkage increases with the increasing immersion time, because more water would spread into ethanol driven by the difference of water concentration inside and outside the hydrogels as increase in immersion time. And the volume shrinkage is generally less than 70%. It should be mentioned that volume shrinkage and the tensile strength changing with soaking time are consistent. For example, the volume shrinkage at 2 h is a bit higher than 1 h. Likewise, the tensile strength of sample immersed for 2 h is just 60 KPa higher than that immersed for 1 h. The volume shrinkage of 4 h increases suddenly compared with 2 h, and the hydrogels of 4 h exhibit a huge increase in tensile strength too. Therefore, the density of the hydrogel's network does have great impact on the strength. The hydrogels with different treatment time in ethanol were soaked into large amount of water for 24 h to study the swelling properties. Fig. 3D shows that the swelling ratio of hydrogels without the treatment in ethanol is 108%, while the swelling ratio of hydrogels after treatment in ethanol for 4 h reach to 300%. The final swelling ratio of the treated hydrogels is higher than that of the pure hydrogel, which is because the initial hydration degree of ethanol-treated hydrogels is lower than the untreated one. The results suggest that the prepared hydrogels are not fully swollen. And the ethanol treatment just changes the network structure by removing the water from the hydrogels and do not affect to the hydrophilicity of the hydrogels.

The dynamic viscoelastic properties of the PAAm-HNT hydrogels

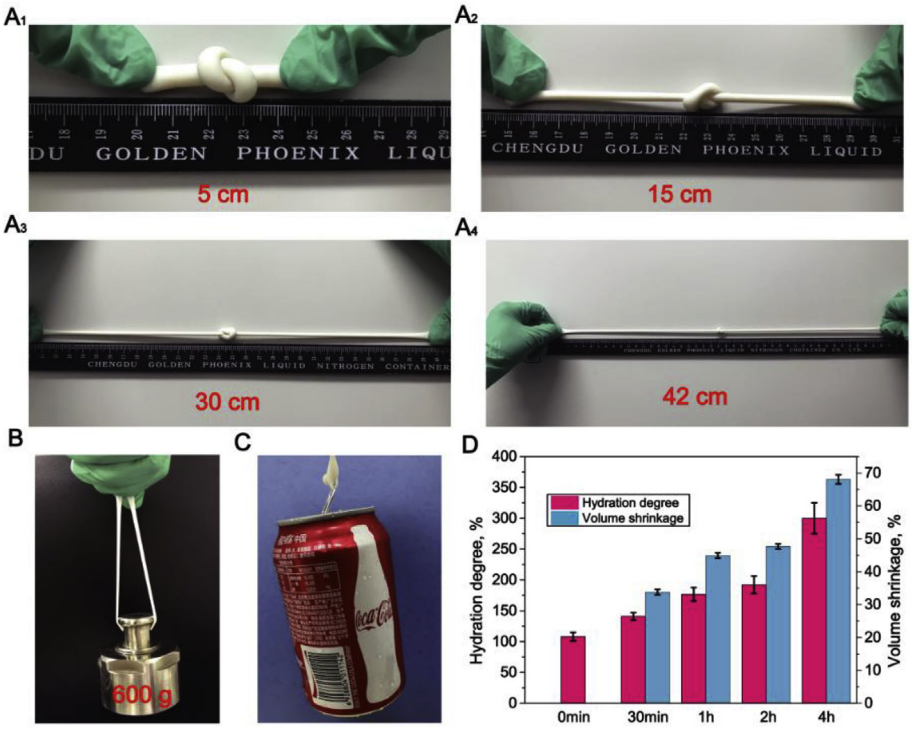

Fig. 3. A_1) The initial length of ethanol treated PAAm-HNT hydrogel under knotting. A_2 to A_4 exhibits the process of knotted hydrogels stretched to 15 cm, 30 cm, and 42 cm respectively. B) 600 g steel block and C) 330 mL Coca Cole was hung from ethanol treated PAAm-HNT hydrogel. D) Swelling ratio and volume shrinkage of PAAm-HNT hydrogel with different ethanol immersion time.

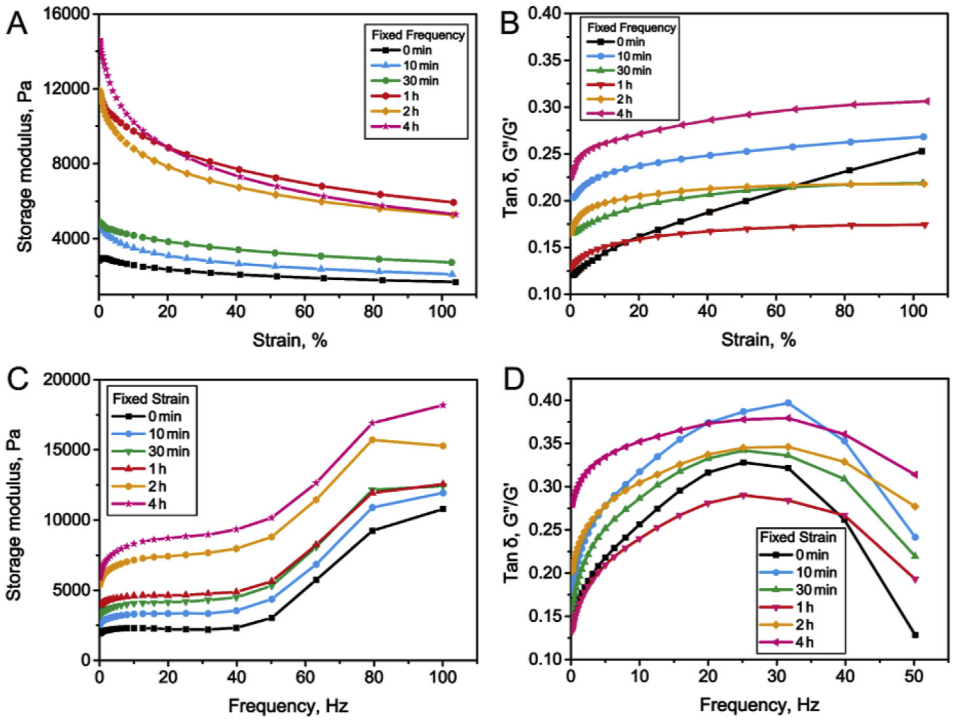

Fig. 4. Rheological properties of PAAm-HNT hydrogel with different ethanol immersion time. A) Storage modulus and B) loss tangent as a function of strain from 0.1% to 100%. C) Storage modulus and D) loss tangent of hydrogels as a function of angular frequency.

were further investigated with a rheometer. As shown in Fig. 4A, the storage modulus substantially increases with the extension of soaking time in ethanol at low strain range, and the storage modulus of the hydrogels increases after being treated in ethanol for 1 h. For example, the G' of hydrogels for 1 h treatment at 1% strain is 11,349 Pa, which is 138% higher than the hydrogels for 30 min treatment. This demonstrates that hydrogels soaked in ethanol overs 1 h achieved better elasticity. In addition, the storage modulus of all the samples decrease with increasing strain, and the decline with treatment time in ethanol over 1 h is more pronounced. The difference among the samples was considered from the formation of different network structures in the hydrogels. i.e. the soft but tight polymer network and the rigid but loose inorganic network. The polymer network is formed by the cross-linked PAAm chains via hydrogen interactions with HNTs and the entanglement of molecular chains, while the inorganic network is formed via the hydrogen bonds and/or electrostatic interaction among the HNTs [42].

The entanglement among PAAm, the interactions between PAAm and HNTs, and the hydrogen bonding within PAAm increase with the extension of soaking time. But for ethanol-soaked hydrogels over 1 h, the loose inorganic network may be slightly damaged by the solvent under stress, which is responsible for the slight decrease in storage modulus. The rheological properties further confirm that the interface strength is indeed enhanced by the treatment in ethanol.

Fig. 4B exhibits Tan δ curve of ethanol-treated hydrogels as a function of strain. Tan δ value of all samples increases with increasing strain. This is owing to the viscous dissipation caused by the hysteretic segment movement and the interface detachment. The hydrogel treated with ethanol for 1 h has minimum Tan δ when the applied strain exceeds 30%. The reason can be explained as follow. The network of the hydrogels treated less than 1 h is relatively loose. Therefore, the segment movement driven by external force is sufficient, leading to greater viscous dissipation. Consequently, the Tan δ of hydrogels treated with 0, 10, and 30 min were all higher than that of hydrogel treated with 1 h. Hydrogels treated with ethanol for a period of more than 1 h have a relatively dense network, so the chain segment movement needs to overcome high viscous resistance, for which the Tan δ of 4 h is the highest. For the hydrogels treated for 1 h, the resistance of chain segment movement is lower than that of 4 h, and segment movement is not as sufficient as that of 10 min, so Tan δ is the lowest.

Fig. 4C exhibits the storage modulus of ethanol-treated hydrogels as a function of angular frequency. At the same frequency, the storage modulus is higher with longer treatment time in ethanol. The extension of soaking time leads to more physical crosslinking points and stronger physical crosslinking strength, which makes it more difficult for segment to move, so the storage modulus increased with the extension of the soaking time. The storage modulus of the hydrogel increases for all samples at relative high frequencies. This is due to that only the mobility of bond length and the bond angle can occur while the movement of the chain segments cannot take place at high frequencies. Fig. 4D exhibits the Tan δ of ethanol-treated gels as a function of angular frequency. For all samples, the Tan δ increases first and then decreases with increasing frequency. At low frequencies, the deformation can keep up with the change of stress, the hysteretic segment movement is small. At high frequencies, the movement of the chain segments cannot take place, resulting in low Tan δ. When the frequencies are at a certain range, the segment can move but can't keep up with the change of stress, and a large hysteresis is observed. Similarly, in the case of frequency less than 40 Hz, the hydrogel soaked in ethanol for 1 h has the lowest loss factor, and the specific reasons has been discussed in Fig. 4B.

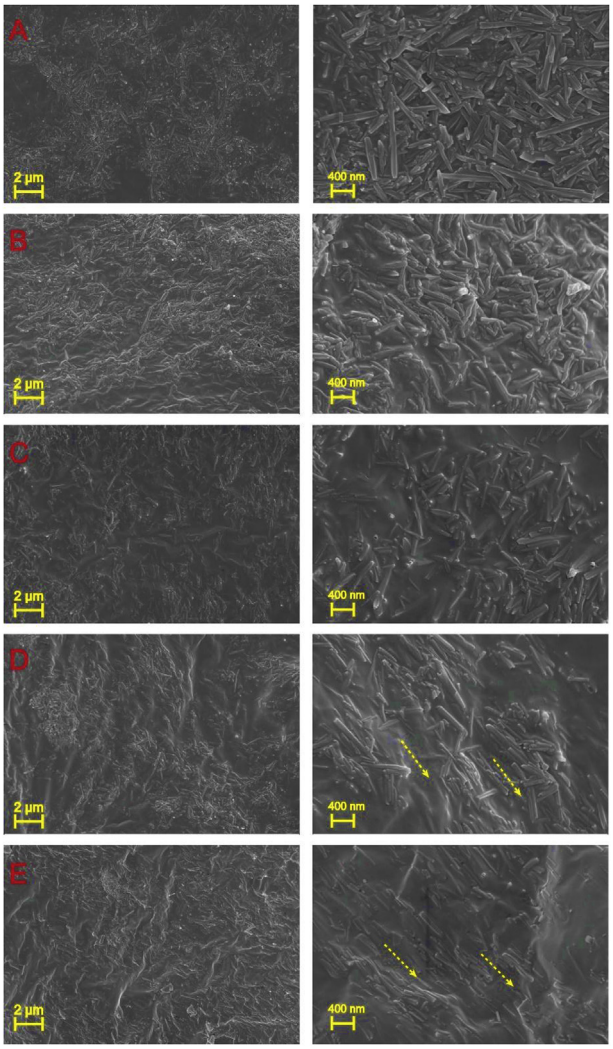

Fig. 6. SEM photos of PAAm-HNT hydrogel after ethanol immersion for A) 0 h, B) 10 min, C) 30 min, D) 1h, E) 4 h and then freeze drying. The magnification on the left is 5000 X while the magnification on the right is 20,000 X.

3.2. Microstructure

From the FTIR spectra of freeze-dried PAAm-HNT hydrogels (Fig. 5A), the characteristic peaks of HNTs can be identified clearly. For example, the peak around 3696 and 3620 cm^{-1} are assigned to the vibration of hydroxyl groups Si–OH and Al–OH respectively. And the peak at 1036 cm^{-1} is ascribed to Si–O–Si stretching vibrations [15]. Aliphatic stretching of CH_2 at 2926 cm^{-1} and the C=O stretching vibration at 1652 cm^{-1} demonstrate the existence of PAAm [44,45]. The XRD pattern result also support the conclusion as shown in Fig. 5B. Compared with the XRD of HNTs powder, the peak location at 12° (001 plane) with a layer spacing of 0.74 nm remains unchanged with the

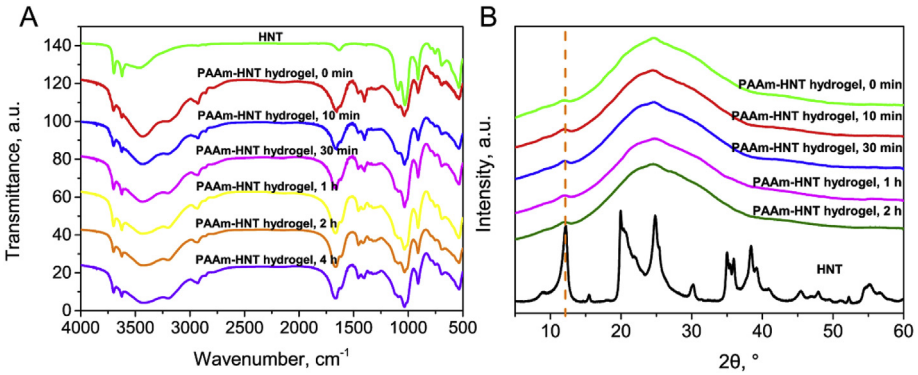

Fig. 5. A) FTIR spectra of PAAm-HNT hydrogel with different ethanol immersion time and HNTs. B) XRD of PAAm-HNT hydrogel with different ethanol immersion time and HNT pattern.

treatment of ethanol, suggesting that the unchanged interlayer spacing. Because the interlayer spacings of HNTs were too small to allow the long PAAm chain to enter, HNTs are not intercalated by PAAm during polymerization and ethanol treatment. This can be explained by that PAAm is polymerized on the surfaces of HNTs but not in the layer spacing.

To further illustrate the effect of ethanol treatment on hydrogel, the microstructure was analyzed by SEM. HNTs exhibit a high aspect ratio with diameter of ~50 nm and length in 400–1500 nm (Fig. S2). The large aspect ratio of HNTs will not lead to the anisotropy of the hydrogels because of their random distribution in hydrogels, as shown in the SEM images in Fig. 6. HNTs display a satisfactory dispersion state and show good interfacial bonding with the matrix, which is attributed to the proper aspect ratio and relatively weak tube–tube interactions of HNTs [46]. It should be noted that less HNTs are exposed on the surface of gels as the soaking time increases. The main reason for this is the embedding effect of PAAm layer on HNTs upon ethanol immersing. Because of the strong interactions between PAAm and HNTs particularly in ethanol solutions, the outer surface of the HNTs is covered with a thick layer of PAAm during the ethanol soaking treatment. This effect makes the HNTs be embeded into the matrix with very blurry interface [42], and consequently the number of exposed HNTs on the surfaces decrease. Also, the interactions between ethanol and PAAm are stronger than the interactions between ethanol and HNTs. Therefore, PAAm chains would move to the surface of the hydrogels and encapsulate HNTs, making the outline of HNTs more blurred. In addition, a directional arrangement of HNTs is found in some regions when the hydrogels are treated with ethanol for more than 1 h, as shown in Fig. 6D and E. We suppose that the polymers adhered on the surface of HNTs have a certain orientation structure during elongation, which may make contributions to the improvement of mechanical properties [42].

3.3. Strain sensor application

The mechanism of the formation of nanocomposite hydrogels and the structure of organic/inorganic network were studied by Haraguchi et al. It showed that KPS, located near the clay surfaces, induced the polymerization. The free radica induced the polymerization of monomer, and clay-brush particles and organic/inorganic networks were formed [47]. Hence, it is supposed that the K^+ ions from KPS may work as conductor, and the K^+ are adsorbed on the outer surface of HNTs since the nanotubes are negatively charged [48]. Upon the tensile strain, the conductivity of the hydrogel changes because K^+ can move with HNTs in the matrix [42]. Fig. 7A shows the relative resistance R/R_0 change as the strain sensors stretched from 0% to 200%. The relative resistance increases with the increasing strain, which is caused by the separation of conductors or the reduction of conductors' contact area under deformation [37]. One can see that the relative resistance in releasing process is much higher than the stretching process, which is due to that the hysteresis of segmental motion hider the reconstruction of the conductive network [49]. In Fig. 7B, the relative resistance of hydrogel rapidly reach to a constant value when strain is remained unchanged, indicating an excellent stability for the strain sensor. Fig. 7C shows the changes in relative resistance R/R_0 of the strain sensors upon 3 tensile-release cycles of 100%, 200%, 300%, and 400% respectively. One can see that the relative resistence curves are repeatable under the same strain cycles. The conductive properties of the hydrogel are also evaluated by linking a complete circuit composed of a LED bulb with PAAm-HNT hydrogels as conductor wire (Fig. 7D). The LED is bright in unstretched state. As the elongation increases, the brightness of the LED decreases gradually. Eventually the LED is estinguished at the strain of 200%. As the elongation gradually decreases from 200%, the brightness of the LED increases. When it returns to the unstretched state, the brightness of the LED is the same as $\mathbf{D_1}$, also suggesting the structure can be recovered after loading-release cycle (Video S1). The similar result is reporeted in previous study [37].

Stress-strain curves of the PAAM-Laponite gels before and after ethanol immersion; SEM of the HNTs without purification; Relative resistance changes versus time for bending and stretching the knee.

Movie S1, The brilliance change of the LED light versus a cyclic strain.

Movie S2, MB dyes absorption by freeze-dried hydrogels.

Supplementary data related to this article can be found at https://doi.org/10.1016/j.compscitech.2019.107701.

All the results above demonstrate the hydrogels have a potential application in strain sensor. Therefore, the research of the conductive hydrogels in wearable devices are designed in present study. In Fig. 8A, the strain sensor is fixed on the latex glove to monitor the human motion of bending and releasing the finger. When the finger is bending, the relative resistance increases. Because the bending is equivalent to the elongation of the strain sensor, which leads to the detachment of the conductor. Similar result can be seen when the strain sensors are used to detect the motion of bending and releasing the elbow (Fig. 8B) and the knee (Fig. S3). More interestingly, the strain sensor can be attached to the soles. The difference of the pace speed can be detected as shown in Fig. 8C and D. Therefore, the strain sensor with a circuit might be designed as a passometer. In the composites, the amount of KPS could affect the conductivity of the final nanocomposite hydrogels. A higher concentration of KPS may lead to a better conductivity but lower detection sensitivity of the hydrogel sensor.

3.4. Dye adsorption

The adsorption ability toward MB by freeze-dried gels was measured and the results are shown in Fig. 9. Fig. 9A, B and C show the appearance of the centrifuge tube with freeze-dried gels immersed in MB solution, filtrate solution after adsorption, and the swelling hydrogels for different adsorption time, respectively. As observed from Fig. 9B and the movie in supporting information (Video S2), the color of solution disappeared as soon as 15 min, and after that the color is slightly changed with prolonged adsorption time. However, there are great differences among the hydrogels as shown in Fig. 9C. The color of the initial freeze-dried gel is beige. Then, the gels are slightly swollen and turn light blue after immersing in the MB solution for 15 min. Finally, the gels are fully swollen and turn to dark blue. From Fig. 9D, it is clearly seen that absorbance of MB solution decreased sharply after the adsorption by the freeze-dried hydrogels. The enlarged curve of adsorption amount and adsorption time is shown in Fig. 9E. At the initial stage (0–2 h), the absorbance decreases with the extension of the adsorption time, which is related to the superior capacity of freeze-dried gels to adsorb the MB dyes. In the middle stage (2–8 h), the absorbance increases slightly compared to 2 h. And in the later stage (> 8 h), the absorbance gradually decreases with prolonged adsorption time and tends to be stable. The increase of absorbance in the middle stage can be attributed to the dissolution of HNTs and PAAm in hydrogel, leading to the desorption of dye and turbidity of solution, which increase the absorbance. In the later stage, the bulk hydrogel resorbs the dissolved substance. This process makes the solution clear and reduces the amount of dye in the solution. Both the hydrogen bonding between PAAm and MB and the coulombic interaction between HNTs and MB contributed to the dye absorption for the nanocomposite hydrogels. Moreover, the capillary effect originated from the hollow structure of HNTs makes the dye absorption more effective.

The adsorption capability (Q_t) and removal efficiency (E) are illustrated in Fig. 9F. The adsorption capacity of the freeze-dried gels reaches to 1 mg/g in 15 min, and there are only slight changes with adsorption time going. For example, the Q_t of 2 h, 4 h, 8 h, 12 h, 20 h, 24 h are 1.02, 1.015, 1.015, 1.027,1.032 and 1.037 mg/g, respectively. Although the adsorption capability is not impressive, the removal efficiency is striking. Within 15 min, the removal efficiency reaches to 96.66%, and it finally reaches to 99.56% after a 24 h. In conclusion, the freeze-dried hydrogels are suitable for the pretreatment of dye

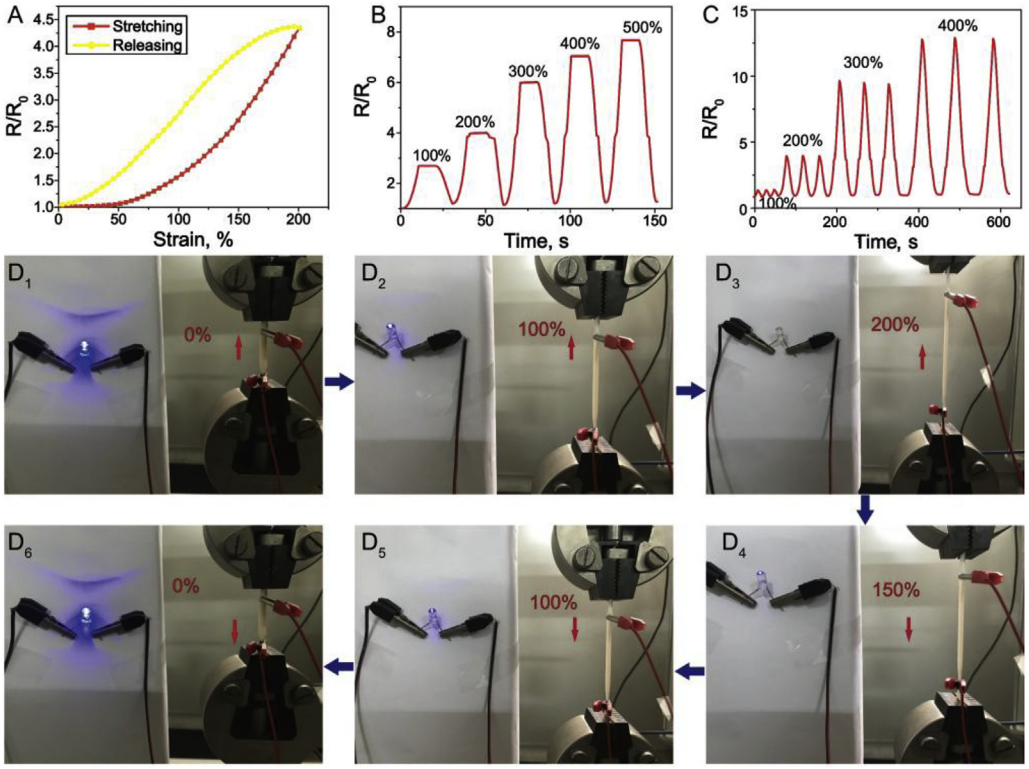

Fig. 7. The performance of ethanol treated PAAm-HNT hydrogel as sensors. A) Relative resistance variation versus a strain change of 0%–200%-0%. B) Relative resistance changes under gradually increasing step strain from 100% to 500%. C) Relative resistance changes as the sensor was streched from 0% to 100%, 200%, 300%, 400% in turn. D) The brightness change of the LED light versus a strain change of 0%–200%-0%.

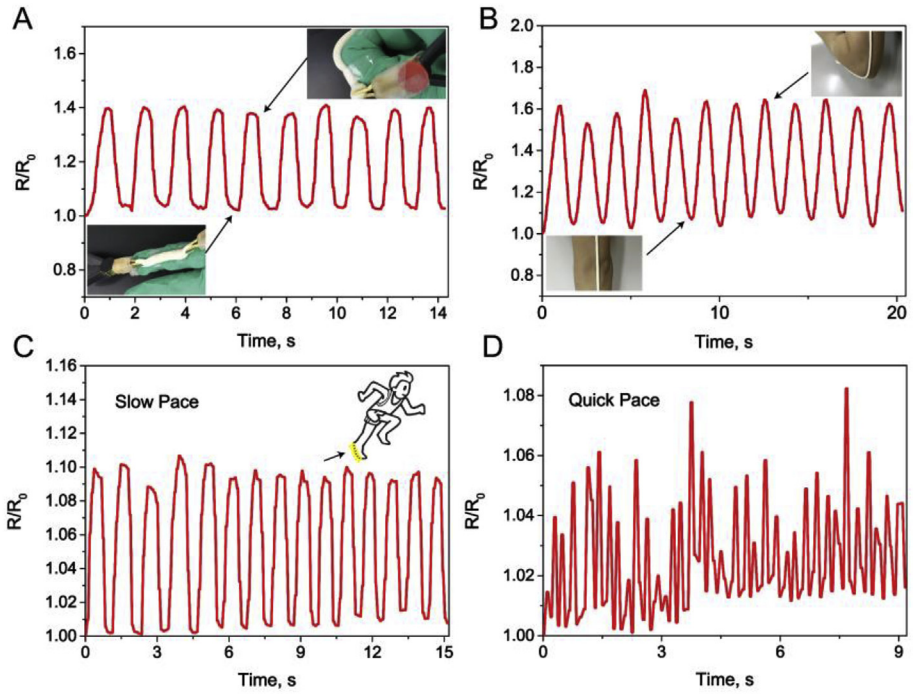

Fig. 8. A feasibility study of ethanol treated PAAm-HNT hydrogel on wearable device. Relative resistance changes versus time for the bending and releasing of A) the index finger, B) the elbow. C) Relative resistance changes versus time for walking in slow pace, the insert showing the gels attached to the sole. D) Relative resistance changes versus time for running in quick pace.

adsorption because of its high removal efficiency with high adsorption capacity.

4. Conclusions

In summary, a simple way to obtain PAAm-HNT hydrogels with high strength and high elasticity is developed by in-situ polymerazation and immersing in ethanol. With immersion in ethanol for 1 h, the tensile strength of the hydrogels significantly increases from 74 KPa to 234 KPa, accompanied by the increase in elongation at break from 885% to 2083%. The ethanol concentration and immersion time have a positively effect on the strength and toughness of the hydrogels. This method can be applied to other system like PAAm-laponite gels. The hydrogel network become dense and an arrangement of the clay tubes is found in the matrix after immersing in ethanol. The K^+ ions from KPS, adsorbed on the outer surface of HNTs, may work as conductor. Upon the tensile strain, the conductivity changed since K^+ ions can move along with the movement of HNTs in the PAAM matrix.

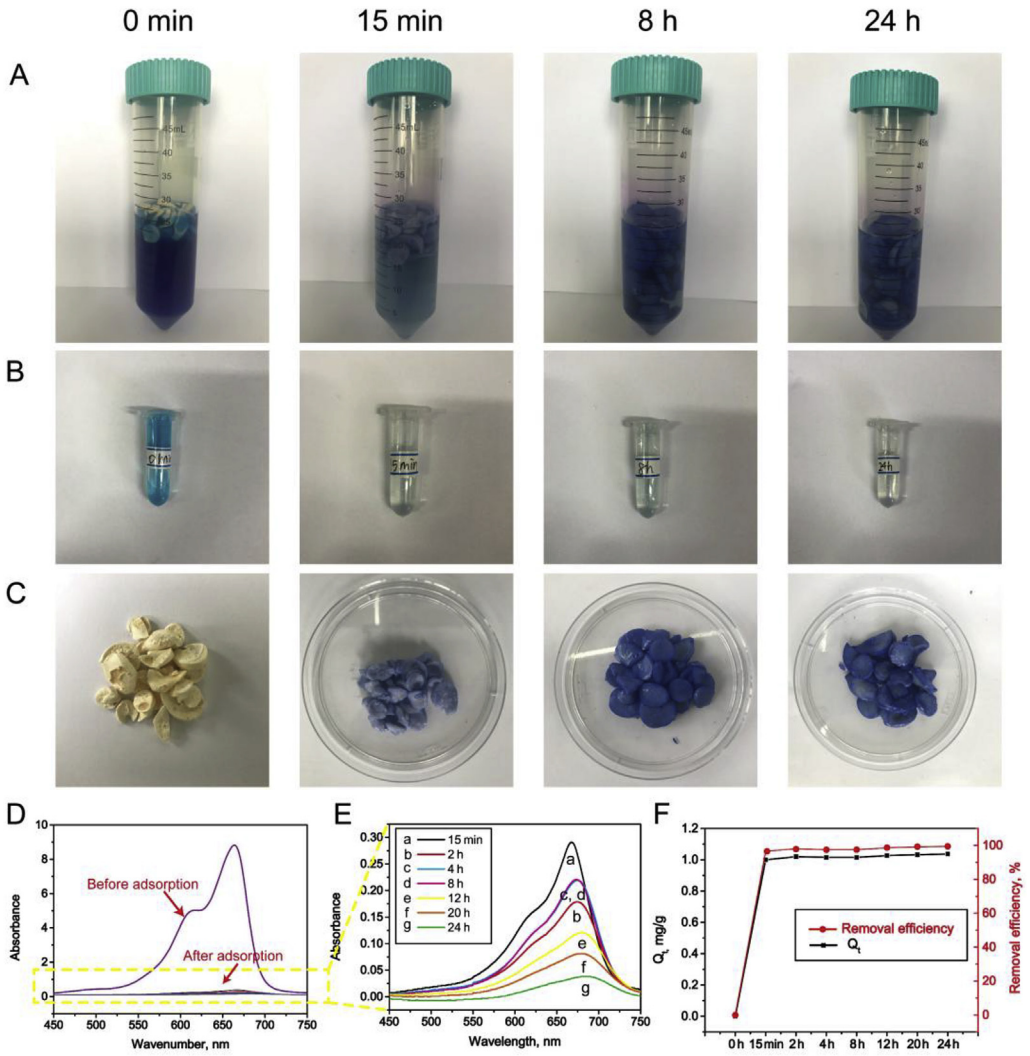

Fig. 9. The dye adsorption performance of freeze-dried PAAm-HNT hydrogel. The comparison A) of the centrifuge tube with freeze-dried hydrogels immersed in MB solution, B) of filtrate, and C) of swelling hydrogels for different adsorption time. D) The UV–Vis spectra of MB solution before and after being adsorbed by freeze-dried hydrogels. E) the enlarged UV–Vis spectra of MB solution after being adsorbed by hydrogels for different hours. F) The change of adsorption capacities and removal efficiency versus absorption time.

Therefore, the composite hydrogels are conductive and can be used as strain sensor, exhibiting good stability and recoverability even under a strain at 400%. The strain sensor made from these hydrogels can sensitively monitor the movement of finger, elbow, knee or even the speed of the pace well. In addition, the freeze-dried gels have a good ability to absorb dyes and show a superior removal efficiency. This work opens a simple, economical, and practical way to synthesze high-strength physically cross-linked composite hydrogel using natural and environmental-friendly nanoparticles, which shows great potentials in wearable devices and environmental restoration.

Notes

The authors declare no competing financial interest.

Acknowledgements

This work was financially supported by National Natural Science Foundation of China (51473069 and 51502113), the Pearl River S and T Nova Program of Guangzhou (201610010026), and the Fundamental Research Funds for the Central Universities (21619102).

Appendix A. Supplementary data

Supplementary data to this article can be found online at https://doi.org/10.1016/j.compscitech.2019.107701.

References

[1] A.M. Mathur, S.K. Moorjani, A.B. Scranton, Methods for synthesis of hydrogel networks: a review, J. Macromol. Sci., Polym. Rev. 36 (2) (1996) 405–430.
[2] X. Xu, A.K. Jha, D.A. Harrington, M.C. Farach-Carson, X. Jia, Hyaluronic acid-based hydrogels: from a natural polysaccharide to complex networks, Soft Matter 8 (12) (2012) 3280–3294.
[3] T. Segura, P.H. Chung, L.D. Shea, DNA delivery from hyaluronic acid-collagen hydrogels via a substrate-mediated approach, Biomaterials 26 (13) (2005) 1575–1584.
[4] A. des Rieux, A. Shikanov, L.D. Shea, Fibrin hydrogels for non-viral vector delivery in vitro, J. Control. Release 136 (2) (2009) 148–154.
[5] M. Ishihara, K. Obara, S. Nakamura, M. Fujita, K. Masuoka, Y. Kanatani, B. Takase, H. Hattori, Y. Morimoto, M. Ishihara, Chitosan hydrogel as a drug delivery carrier to control angiogenesis, J. Artif. Organs 9 (1) (2006) 8–16.
[6] I. Tomatsu, A. Hashidzume, A. Harada, Photoresponsive hydrogel system using molecular recognition of α-cyclodextrin, Macromolecules 38 (12) (2005) 5223–5227.
[7] J. Carvalho, C. Gonçalves, A.M. Gil, F.M. Gama, Production and characterization of a new dextrin based hydrogel, Eur. Polym. J. 43 (7) (2007) 3050–3059.
[8] B. Ye, S. Zhang, R. Li, L. Li, L. Lu, C. Zhou, An in-situ formable and fibrils-reinforced polysaccharide composite hydrogel by self-crosslinking with dual healing ability,

Compos. Sci. Technol. 156 (2018) 238–246.
[9] F. Li, G. Zhang, Y. Xia, Z. Wang, H. Jiang, X. Feng, Y. Zhang, M. Liu, H. Li, Hierarchically crosslinked ionic nanocomposite hydrogels with ultrahigh mechanical properties for underwater bioinspired capturing device, Compos. Sci. Technol. 165 (2018) 339–346.
[10] Y. Wang, C. Song, X. Yu, L. Liu, Y. Han, J. Chen, J. Fu, Thermo-responsive hydrogels with tunable transition temperature crosslinked by multifunctional graphene oxide nanosheets, Compos. Sci. Technol. 151 (2017) 139–146.
[11] K. Haraguchi, T. Takehisa, Nanocomposite hydrogels: a unique organic–inorganic network structure with extraordinary mechanical, optical, and swelling/de-swelling properties, Adv. Mater. 14 (16) (2002) 1120–1124.
[12] C.H. Yang, M.X. Wang, H. Haider, J.H. Yang, J.-Y. Sun, Y.M. Chen, J. Zhou, Z. Suo, Strengthening alginate/polyacrylamide hydrogels using various multivalent cations, ACS Appl. Mater. Interfaces 5 (21) (2013) 10418–10422.
[13] M. Liu, Z. Jia, D. Jia, C. Zhou, Recent advance in research on halloysite nanotubes-polymer nanocomposite, Prog. Polym. Sci. 39 (8) (2014) 1498–1525.
[14] Y. Lvov, W. Wang, L. Zhang, R. Fakhrullin, Halloysite clay nanotubes for loading and sustained release of functional compounds, Adv. Mater. 28 (6) (2016) 1227–1250.
[15] K. Feng, G.-Y. Hung, J. Liu, M. Li, C. Zhou, M. Liu, Fabrication of high performance superhydrophobic coatings by spray-coating of polysiloxane modified halloysite nanotubes, Chem. Eng. J. 331 (2018) 744–754.
[16] M. Liu, Y. Chang, J. Yang, Y. You, R. He, T. Chen, C. Zhou, Functionalized halloysite nanotube by chitosan grafting for drug delivery of curcumin to achieve enhanced anticancer efficacy, J. Mater. Chem. B 4 (13) (2016) 2253–2263.
[17] J. Yang, Y. Wu, Y. Shen, C. Zhou, Y.-F. Li, R.-R. He, M. Liu, Enhanced therapeutic efficacy of doxorubicin for breast cancer using chitosan oligosaccharide-modified halloysite nanotubes, ACS Appl. Mater. Interfaces 8 (40) (2016) 26578–26590.
[18] M. Massaro, A. Campofelice, C.G. Colletti, G. Lazzara, R. Noto, S. Riela, Functionalized halloysite nanotubes: efficient carrier systems for antifungine drugs, Appl. Clay Sci. 160 (2018) 186–192.
[19] M. Liu, R. He, J. Yang, W. Zhao, C. Zhou, Stripe-like clay nanotubes patterns in glass capillary tubes for capture of tumor cells, ACS Appl. Mater. Interfaces 8 (12) (2016) 7709–7719.
[20] M. Zhao, P. Liu, Adsorption behavior of methylene blue on halloysite nanotubes, Microporous Mesoporous Mater. 112 (1–3) (2008) 419–424.
[21] W. Jinhua, Z. Xiang, Z. Bing, Z. Yafei, Z. Rui, L. Jindun, C. Rongfeng, Rapid adsorption of Cr (VI) on modified halloysite nanotubes, Desalination 259 (1–3) (2010) 22–28.
[22] L. Lisuzzo, G. Cavallaro, P. Pasbakhsh, S. Milioto, G. Lazzara, Why does vacuum drive to the loading of halloysite nanotubes? The key role of water confinement, J. Colloid Interface Sci. 547 (2019) 361–369.
[23] G.S. Machado, F. Wypych, S. Nakagaki, Immobilization of metalloporphyrins into nanotubes of natural halloysite toward selective catalysts for oxidation reactions, J. Mol. Catal. A Chem. 283 (1) (2008) 99–107.
[24] G. Lazzara, G. Cavallaro, A. Panchal, R. Fakhrullin, A. Stavitskaya, V. Vinokurov, Y. Lvov, An assembly of organic-inorganic composites using halloysite clay nanotubes, Curr. Opin. Colloid Interface Sci. 35 (2018) 42–50.
[25] W.U. Wei, W.U. Pengjun, H.E. Ding, X. Cao, N. Zhou, Application progress of halloysite nanotube in polymer nanocomposites, Chem. Ind. Eng. Prog. 30 (12) (2011) 2647-2636.
[26] T.S. Gaaz, A.B. Sulong, A.A.H. Kadhum, M.H. Nassir, A.A. Alamiery, Optimizing injection molding parameters of different halloysites type-reinforced thermoplastic polyurethane nanocomposites via taguchi complemented with ANOVA, Materials 9 (11) (2016) 947.
[27] N.F.A. Sharif, Z. Mohamad, M.U. Wahit, Novel epoxidized natural rubber toughened polyamide 6/halloysite nanotubes nanocomposites, J. Polym. Res. 19 (1) (2012) 9749.
[28] C. Huang, Y. Sun, S. Xiang, P. Ma, W. Dong, M. Chen, J. University, Enhanced mechanical strength of double-network hydrogels in the presence of halloysite nanotubes, Rare Metal Mater. Eng. 43 (2014) 200–204.
[29] B. Huang, M. Liu, C. Zhou, Cellulose–halloysite nanotube composite hydrogels for curcumin delivery, Cellulose 24 (7) (2017) 2861–2875.
[30] M. Liu, Y. Zhang, J. Li, C. Zhou, Chitin-natural clay nanotubes hybrid hydrogel, Int. J. Biol. Macromol. 58 (7) (2013) 23–30.
[31] B. Huang, M. Liu, Z. Long, Y. Shen, C. Zhou, Effects of halloysite nanotubes on physical properties and cytocompatibility of alginate composite hydrogels, Mater. Sci. Eng. C 70 (2017) 303–310.
[32] M.A. Bonifacio, P. Gentile, A.M. Ferreira, S. Cometa, E.D. Giglio, Insight into halloysite nanotubes-loaded gellan gum hydrogels for soft tissue engineering applications, Carbohydr. Polym. 163 (2017) 280–291.
[33] M. Amjadi, K.U. Kyung, I. Park, M. Sitti, Stretchable, skin-mountable, and wearable strain sensors and their potential applications: a review, Adv. Funct. Mater. 26 (11) (2016) 1678–1698.
[34] X.G. Xin, G.T. Fei, B.F. Wen, F. Ming, D.G. Xu, B.N. Zhong, D.Z. Li, Flexible strain sensor with high performance based on PANI/PDMS films, Org. Electron. 47 (2017) 51–56.
[35] J.A. Rogers, T. Someya, Y. Huang, Materials and mechanics for stretchable electronics, Science 327 (5973) (2010) 1603–1607.
[36] Z. Lei, Q. Wang, S. Sun, W. Zhu, P. Wu, A bioinspired mineral hydrogel as a self-healable, mechanically adaptable ionic skin for highly sensitive pressure sensing, Adv. Mater. 29 (22) (2017) 1700321.
[37] G. Cai, J. Wang, K. Qian, J. Chen, S. Li, P.S. Lee, Strain sensors: extremely stretchable strain sensors based on conductive self-healing dynamic cross-links hydrogels for human-motion detection, Adv. Sci. 4 (2) (2016) 1600190.
[38] Y.-F. Fu, Y.-Q. Li, Y.-F. Liu, P. Huang, N. Hu, S.-Y. Fu, High-performance structural flexible strain sensors based on graphene-coated glass fabric/silicone composite, ACS Appl. Mater. Interfaces 10 (41) (2018) 35503–35509.
[39] C.L. Choong, M.B. Shim, B.S. Lee, S. Jeon, D.S. Ko, T.H. Kang, J. Bae, S.H. Lee, K.E. Byun, J. Im, Highly stretchable resistive pressure sensors using a conductive elastomeric composite on a micropyramid array, Adv. Mater. 26 (21) (2014) 3451–3458.
[40] Z. Wang, J. Chen, Y. Cong, H. Zhang, T. Xu, L. Nie, J. Fu, Ultrastretchable strain sensors and arrays with high sensitivity and linearity based on super tough conductive hydrogels, Chem. Mater. 30 (21) (2018) 8062–8069.
[41] X. Jing, H.-Y. Mi, Y.-J. Lin, E. Enriquez, X.-F. Peng, L.-S. Turng, Highly stretchable and biocompatible strain sensors based on mussel-inspired super-adhesive self-healing hydrogels for human motion monitoring, ACS Appl. Mater. Interfaces 10 (24) (2018) 20897–20909.
[42] M. Liu, W. Li, J. Rong, C. Zhou, Novel polymer nanocomposite hydrogel with natural clay nanotubes, Colloid Polym. Sci. 290 (10) (2012) 895–905.
[43] N. Yuan, L. Xu, H. Wang, Y. Fu, Z. Zhang, L. Liu, C. Wang, J. Zhao, J. Rong, Dual physically cross-linked double network hydrogels with high mechanical strength, fatigue resistance, notch-insensitivity, and self-healing properties, ACS Appl. Mater. Interfaces 8 (49) (2016) 34034–34044.
[44] J. Jang, H. Park, Formation and structure of polyacrylamide–silica nanocomposites by sol–gel process, J. Appl. Polym. Sci. 83 (8) (2002) 1817–1823.
[45] T. Liu, F. Xue, E. Ding, Cellulose nanocrystals grafted with polyacrylamide assisted by macromolecular RAFT agents, Cellulose 23 (6) (2016) 3717–3735.
[46] M. Liu, B. Guo, M. Du, X. Cai, D. Jia, Properties of halloysite nanotube–epoxy resin hybrids and the interfacial reactions in the systems, Nanotechnology 18 (45) (2007) 455703.
[47] K. Haraguchi, H.-J. Li, K. Matsuda, T. Takehisa, E. Elliott, Mechanism of forming organic/inorganic network structures during in-situ free-radical polymerization in PNIPA − clay nanocomposite hydrogels, Macromolecules 38 (8) (2005) 3482–3490.
[48] Y. Lin, X. Wang, J. Liu, J.D. Miller, Natural halloysite nano-clay electrolyte for advanced all-solid-state lithium-sulfur batteries, Nano Energy 31 (2017) 478–485.
[49] Y. Liu, F. Wu, X. Zhao, M. Liu, High-performance strain sensors based on spirally structured composites with carbon black, chitin nanocrystals, and natural rubber, ACS Sustain. Chem. Eng. 6 (8) (2018) 10595–10605.